THE JOURNAL OF PHYSICAL CHEMISTRY C
A JOURNAL OF THE AMERICAN CHEMICAL SOCIETY

pubs.acs.org/JPCC Article

Understanding Water–Zeolite Interactions: On the Accuracy of Density Functionals

Katarina Stanciakova, Jaap N. Louwen, Bert M. Weckhuysen, Rosa E. Bulo, and Florian Göltl*

Cite This: *J. Phys. Chem. C* 2021, 125, 20261–20274 Read Online

ABSTRACT: Water is ubiquitous in zeolite catalysis, and electronic structure calculations play a crucial role in arriving at an atomistic understanding of water–zeolite interactions. However, a critical evaluation of the performance of different electronic structure methods in describing the interactions between water and zeolites is still missing. Here, we model the adsorption of one water molecule in all-silica chabazite (CHA) and of one and two water molecules in the acidic zeolite SSZ-13 using different electronic structure methods, which include 11 density functional theory (DFT)-based methods and two post Hartree–Fock (HF) methods, namely, the random phase approximation (RPA) and second-order Møller–Plesset (MP2) perturbation theory. We find that all DFT functionals lead to similar structures as long as water is strongly coordinated to the adsorption site, but adsorption energies vary in a range of 50 kJ/mol between the used methods. Subsequently, we use *ab initio* molecular dynamics calculations to show that all methods reproduce the experimentally observed hydrophobicity of purely siliceous zeolites. Comparing DFT energetics with RPA and MP2 calculations shows that PBE and revPBE-D3 adsorption energies show the best agreement with RPA, while BEEF–vdW agrees the best with MP2 results. At the same time, the performance of PBE functional without any dispersion correction is less consistent with respect to different adsorption sites (BAS, LAS, or the zeolite wall of all-silica CHA) and the BEEF–vdW functional fails to reproduce relative stabilities of the protonation sites. For the adsorption of two water molecules, most methods agree on the formation of a protonated water dimer, and only vdW-DF, vdW-DF2, and BEEF–vdW prefer the formation of a neutral complex. Based on these results, we suggest using the revPBE-D3 functional model water adsorption in purely siliceous or protonated zeolites since it can correctly capture covalent and dispersion interactions, is computationally efficient, correctly predicts the formation of a positively charged water dimer, and is able to closely reproduce adsorption energies calculated at the RPA or MP2 level of theory.

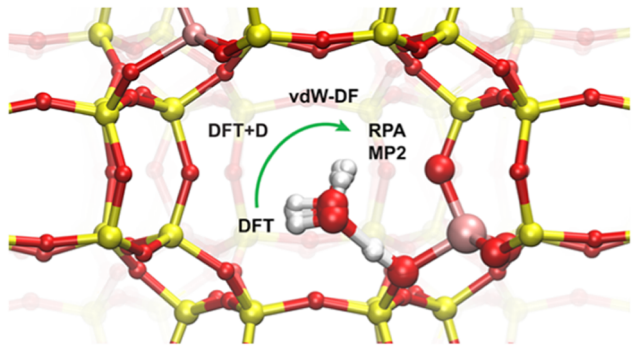

I. INTRODUCTION

Zeolites are nanoporous, crystalline materials, which are mainly composed of Si, Al, and O atoms. In their purely siliceous form, zeolites are relatively inert, but the framework can be chemically functionalized by substituting a Si atom for an Al atom. Since Al has one less valence electron, a local negative charge is required to saturate all bonds to the surrounding O atoms, which is then compensated by the presence of a cation. This cation can be a Brønsted acid site proton (BAS) or a metallic Lewis acid site (LAS), and depending on the nature of the charge compensating cation, zeolites have a broad range of applications in catalysis, separations, or adsorption.[1,2] The performance of a given zeolite material is closely connected to the type and chemical environment of the active center. At the same time, in many of these processes, water is present, which also directly impacts catalytic performance. It has been shown to directly coordinate to (or solvate) active centers such as BASs or transition-metal ions (*e.g.*, Cu), or, given the right conditions, dealuminate the zeolite framework.[3−5] Hence, a detailed understanding of the interactions between water and active sites in the zeolite, as well as the zeolite framework, is required.

Characterization of water–zeolite interactions has, therefore, been an area of intense investigation. Water adsorption on the BAS and formation of protonated water clusters, such as hydronium ions, have been studied using many spectroscopic techniques, in particular, Fourier transform infrared (FT-IR) and NMR spectroscopy.[6,7] Studies on large zeolite ZSM-5 crystals provided detailed insights into the impact of water on the zeolite integrity, which can be significantly impaired at elevated temperatures due to water-induced zeolite dealumination.[8,9] Novel zeolite applications, such as zeolite-

Received: May 14, 2021
Published: September 8, 2021

https://doi.org/10.1021/acs.jpcc.1c04270
J. Phys. Chem. C 2021, 125, 20261–20274

catalyzed biomass conversion, involve water formation or require an aqueous environment.[10] In these cases, the presence of water alters zeolite catalytic activity and stability.[11−15] A dramatic structural collapse of the zeolite framework has been observed for zeolites in the presence of supercritical water; however, this phenomenon is still poorly understood.[11,16]

Despite large interest, a detailed understanding of zeolite−water interactions from an experimental perspective alone remains challenging. Typically, a distribution of active sites and defects is present in a realistic zeolite structure, and all parts of this distribution will interact differently with water and lead to different water arrangements. The complexity of this distribution and potential water arrangements in many cases renders an unambiguous deconvolution of experimental results with respect to all possible motifs impossible.

Due to these limitations, electronic structure calculations have started to play an ever more important role in understanding zeolite−water interactions, in particular, and zeolite catalysis in general.[17,18] For example, De Wispelaere et al. used molecular simulations together with *in situ* spectroscopy to probe the effect of water on the methanol-to-olefin (MTO) process. The authors found that during the reaction water molecules compete with methanol molecules for adsorption on the BASs, which attenuates coke formation, thus rationalizing improved catalyst performance.[19] Mechanistic insights into water-induced zeolite dealumination have been gained from a series of recent density functional theory (DFT) investigations.[20−24] It has been shown that the water attack starts by the adsorption on the Al atom (LAS) and the process is catalyzed by multiple water molecules, leading to various reaction pathways.[20,22]

At the same time, the accurate description of the adsorption of small molecules in zeolites using the most commonly applied electronic structure methods is difficult. These difficulties are directly related to the interactions between molecules and their zeolitic hosts. On the one hand, molecules in confined spaces can form chemical bonds with adsorption sites, which are determined by the local charge density between the adsorption site and molecule. On the other hand, molecules are also exposed to dispersion interactions with the zeolite framework, which are nonlocal in nature. The most used method in electronic structure calculations, namely, DFT in its general gradient approximation (GGA), is a semilocal method, which, in principle, is unable to capture nonlocal dispersion interactions.

Significant effort has been invested to remedy these shortcomings, and, in particular, two methods have been proven to be successful. In one approach, an attractive two-body force field is added on top of the forces obtained from density functional theory (DFT-D). Several ways to calculate the force field parameters have been suggested, and up until today, methods developed by Grimme et al., which are either based on average interaction parameters for each element (DFT-D2)[25] or are varied with the bonding environment of each atom (DFT-D3),[26] are highly popular in the field. Empirical coefficients have been derived for a large range of DFT functionals, which include GGA functionals and hybrid functionals such as the B3LYP functional.[27−30] A different strategy was suggested by Dion et al., who introduced a nonlocal correlation term, which depends on the charge densities at two points (vdW-DF).[31] Klimeš et al. found that the performance of vdW-DF is crucially dependent on the GGA exchange term included in the functional and tested the performance of a variety of functional forms, such as optB88-vdW (DFT-vdW in general).[32] Additionally, vdW-DF has been refined by Lee et al. (vdW-DF2),[33] and Wellendorff et al. used a machine learning-based optimization algorithm to optimize the exchange term for vdW-DF2, which led to the BEEF−vdW functional.[34] Another computationally less expensive nonlocal vdW functional is the VV10 functional[35] and its revised version (rVV10).[36] These methods are optimized for periodic boundary condition calculations and have been shown to outperform earlier approaches in the description of weakly bound complexes.

At the same time, understanding the performance of these functionals in describing the adsorption of small molecules in zeolites is notoriously difficult. This is related to two main factors in comparing experimental and theoretical results: (i) reliable experimental information, which shows the adsorption strength of exactly one molecule to one well-defined active site, is difficult to obtain and (ii) small molecules adsorbed into zeolite pores retain significant amounts of translational entropy, which makes the calculation of free energies of adsorption, which can be directly compared to experimental results, more difficult.

Another way to assess the performance of DFT-based methods is the comparison to higher-level methods, such as the second-order Møller−Plesset perturbation theory (MP2) or the adiabatic-connection-fluctuation-dissipation-theorem in its random phase approximation (RPA).[37−40] These post Hartree−Fock (HF) methods calculate the correlation energy by considering occupied and unoccupied orbitals and are intrinsically able to capture all local and nonlocal molecule−zeolite interactions.[41] RPA and MP2 have been used to study alkane adsorption,[42,43] hydrocarbon conversions,[44,45] the conversion of biomass,[46] MTO reactions,[47] the conversion of methane to methanol over Fe-oxo sites in zeolites,[48] and the stability of different Cu sites in zeolites.[49] In particular, the calculation of adsorption energies of small molecules in zeolite SSZ-13, the high silica form of zeolite chabazite (CHA), is feasible at MP2 and RPA levels and the results can be used as reference values for other electronic structure calculations.[42,43,50]

Here, we calculate the adsorption energies of one water molecule in three different adsorption configurations: adsorption into the cavity of purely silicious chabazite (CHA) and adsorption to the BAS and to the LAS of the Al atom in the H-form of zeolite SSZ-13. Additionally, we investigate the adsorption of two water molecules in the H-form of zeolite SSZ-13. We use various DFT-based methods (PBE, PBE-D2, PBE-D3, revPBE, revPBE-D3, vdW-DF, optB88-vdW, vdW-DF2, and BEEF−vdW, rVV10), the hybrid functional B3LYP-D3, and the post-HF methods MP2 and RPA. We optimize the structures at the DFT level and subsequently report adsorption strengths of water to all possible adsorption sites. Finally, we compute temperature-dependent adsorption free energies in siliceous zeolite SSZ-13 using *ab initio* molecular dynamics (AIMD) simulations. We then critically evaluate the performance of the DFT-based methods with respect to RPA and experimental observations and discuss how well these methods are able to describe this specific adsorption process.

II. METHODS

II.I. Zeolite Model. In this study, we investigate the adsorption of water in the all-silica CHA and in the H-form of

https://doi.org/10.1021/acs.jpcc.1c04270
J. Phys. Chem. C 2021, 125, 20261−20274

zeolite SSZ-13, which has the chabazite framework. The rhombohedral unit cell of chabazite consists of 12 symmetrically equivalent tetrahedral sites (T-sites) occupied by either Si or Al atoms, each surrounded by four symmetrically different oxygen atoms labeled as O1 to O4.[51] The O1 site is in the four-membered ring (4MR) on the side of the hexagonal prism, O2 belongs to one 4MR, one 6MR, and one 8MR; O3 belongs to two 4MRs and one 6MR; and finally, O4 is located between two hexagonal prisms (Figure 1). The introduction of Al induces an electron deficiency in the framework, which is compensated for by the presence of a hydrogen atom bonded to a neighboring oxygen atom forming a (Si−O(H)−Al) BAS. As an example, the structure of zeolite H-SSZ-13 with a proton bonded in the O1 position is shown in Figure 1.

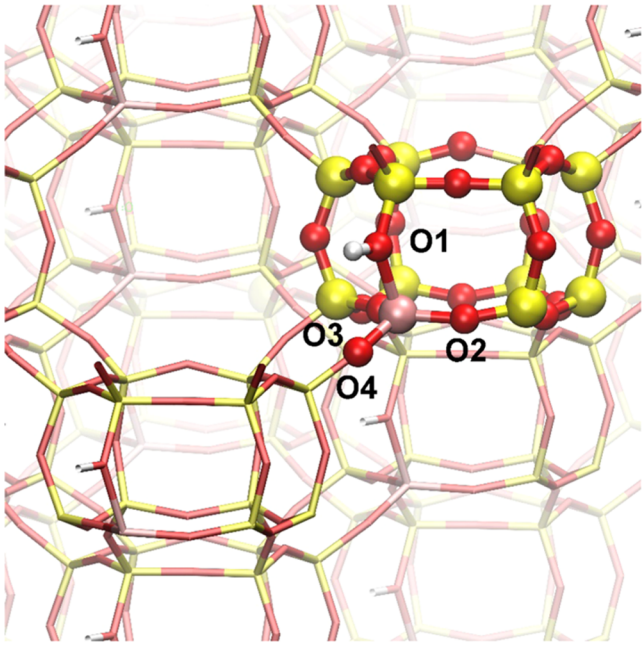

Figure 1. Framework structure of zeolite SSZ-13 with the chabazite (CHA) topology. The unit cell contains 36 atoms of which 12 are crystallographically equal T-sites occupied by either Si or Al atom surrounded by four different oxygen atoms (O1−O4). Oxygen atoms are displayed in red, silica atoms in yellow, the aluminum atom in pink, and hydrogen in white color.

All calculations were carried out using periodic boundary conditions for a single primitive unit cell of the CHA zeolite framework, and we relied on lattice constants optimized using the PBE functional and a TZV2P basis set. As shown in Tables S1 and S2 of the Supporting Information (SI), the choice of the XC functional for the cell optimization has only a negligible influence on the results. The relaxed unit cell parameters for the all-silica CHA and the H-form of zeolite SSZ-13 model were $a = b = c = 9.309$ Å, $\alpha = \beta = \gamma = 93.92°$, and $a = 9.388$ Å, $b = 9.364$ Å, $c = 9.342$ Å, $\alpha = 93.56°$, $\beta = 94.01°$, $\gamma = 94.41°$, corresponding to unit cell volumes 800.78 and 814.85 Å^3, respectively.

A single water molecule can be adsorbed in two different locations around the active site, *i.e.*, bonded to the BAS (the proton) or the LAS (the Al atom), as illustrated in Scheme 1. In this work, we have systematically explored the adsorption of one water molecule on either the BAS or the LAS. We have studied these adsorption processes for all possible protonation sites, which results in eight different structures for acidic SSZ-13. Additionally, we studied adsorption of water in the all-silica CHA, in which water is physisorbed, as well as the simultaneous adsorption of two water molecules. In this context, multiple water−zeolite complexes have been considered in the literature.[22] Here, we focus on two of these complexes, namely, the formation of a water dimer interacting with the acidic proton and a situation where the proton is donated to the water molecules and a positively charged $H_5O_2^+$ dimer is formed (Scheme 1).

II.II. Computational Details. All structure optimizations were performed using periodic boundary conditions using the Gaussian and plane wave method,[52] as implemented in version 6.1 of CP2K software,[53] with PBE-Goedecker−Teter−Hutter (GTH) pseudopotentials.[54] The target accuracy of the self-consistent SCF cycle was set to 10^{-7} charge units and the plane wave cutoff to 900 Ry, while a relative cutoff of 50 Ry was used for the mapping of Gaussians on multigrid levels. All calculations were performed using only the Γ-point in *k*-space.

Adsorption energies were computed using the following functionals: PBE,[55] PBE-D2,[25,55] PBE-D3,[26,55] revPBE,[56] revPBE-D3,[26,56] vdW-DF,[31] vdW-DF2,[33] optB88-vdW,[32] BEEF−vdW,[34] rVV10,[36] and B3LYP-D3[27−30] and compared against RPA and MP2 adsorption energies. Following the original definition of VV10, the full exchange−correlation energy in the rVV10 functional has been obtained by combining the nonlocal correlation of VV10 with the refitted Perdew−Wang exchange functional (rPW86)[57] and PBE correlation.[35] For all calculations, Grimme's D3 correction with zero damping was used. For DFT calculations, the TZV2P MOLOPT basis set was used, while for MP2 and RPA, we have used the RI scheme implemented within CP2K using valence-only correlation consistent-type Gaussian basis sets, namely, cc-TZVP for Al and Si atoms and cc-QZVP for H and O atoms, with auxiliary RI functions of the same quality.[58−60] For computing of the Hartree−Fock exchange in the B3LYP-

Scheme 1. Schematic Representation of Water−Zeolite Complexes upon Water Adsorption on the BAS (the Proton A) or the LAS (B) and Simultaneous Adsorption of Two Water Molecules on the BAS, Which Can Result in the Formation of Neutral Water Dimer Adsorbed on the BAS (C) or the Formation of Charged $H_5O_2^+$ Dimer (D)

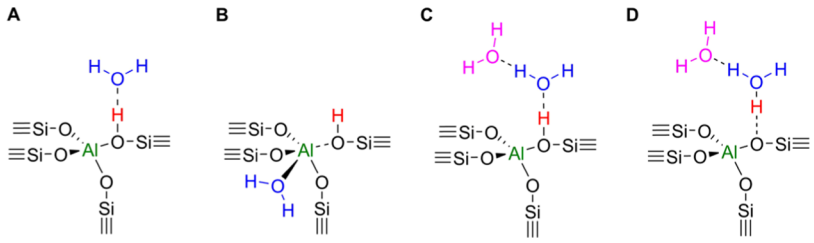

https://doi.org/10.1021/acs.jpcc.1c04270
J. Phys. Chem. C 2021, 125, 20261−20274

D3 functional, we used the auxiliary density matrix method (ADMM)[61] with the aug-pFIT3 auxiliary basis sets. The B3LYP-D3, RPA, and MP2 calculations were performed on top of the geometries optimized using the PBE-D3 functional. The dependence of adsorption energies on the input structures was tested for the H-SSZ-13 model and the O1 protonation site, for which we have recalculated the adsorption energies using structures optimized by all tested functionals. The Coulomb integrals in HF exchange were described using the truncated Coulomb operator with a truncation radius equal to 4.5 Å (approximately one-half of the simulation cell). Subsequently, all GGA calculations were subjected to the basis set superposition-error (BSSE) correction using the counterpoise correction. All convergence tests are summarized in Section S2 and Tables S3−S7. The convergence of the adsorption energies with respect to the basis set is summarized in Table S3 of the SI. In Tables S4 and S5 of the SI, BSSE-corrected and BSSE-uncorrected adsorption energies for all tested structures and functionals are given. The adsorption energies of MP2 and RPA calculations were extrapolated to complete basis set limit (CBS) with the cubic interpolation formula[62−64]

$$E_X = E_{X\to\infty} + AX^{-3} \tag{1}$$

where X is the cardinal number of the basis set and $E_{X\to\infty}$ is the energy in the CBS limit, and A represents a slope of the linear fit, which is used to obtain $E_{X\to\infty}$. X-values of 3.0 and 3.7 for cc-TZVP and combined cc-TZVP/cc-QZVP basis sets were used. The value 3.7 has been chosen based on the ratio between the number of H and O atoms treated on the cc-QZVP level and Si and Al atoms treated on the cc-TZVP level. The reliability of this formula has been previously confirmed for both RPA and MP2 methodologies,[65] as well as correlation consistent Gaussian basis sets.[58] RPA and MP2 adsorption energies computed using both cc-TZVP and cc-TZVP/cc-QZVP basis sets and their extrapolation to CBS limit are tabulated in Table S6 of the SI. Example input files for RI-MP2 and RI-RPA calculations can be found in the SI, Section S6.

To couple our results with experimental observations, we perform *ab initio* molecular dynamics (AIMD) simulations and compute temperature-corrected internal and Helmholtz free energies based on the procedure previously used by Göltl et al.[66] A detailed explanation of this approach applied here is given in the Supporting Information, Section S4.1. We focus on the adsorption of one water molecule in all-silica CHA, which is closely correlated to the experimentally observed hydrophobicity. AIMD calculations were performed in the NVT ensemble at room temperature (298 K), using the revPBE-D3 functional and the same settings as for static DFT calculations, except that the target accuracy of the self-consistent SCF cycle was set to 10^{-5} charge units. The system was initially equilibrated for 3 ps, which was followed by a 10 ps production run with a time step of 0.5 fs. Next, we approximated temperature-dependent adsorption energies of other methods using the correction obtained from AIMD at the revPBE-D3 level

$$U^x(T) = E^X(0\ \mathrm{K}) + U^{r\mathrm{evPBE-D3}}(T) - E^{\mathrm{revPBE-D3}} \tag{2}$$

where $U^x(T)$ indicates the temperature-dependent internal energy, X refers to the method of interest such as RPA or PBE, and E^X is the energy obtained from static DFT calculations. Finally, these values were used to estimate Helmholtz free energies $A^X(T)$. For more details, the reader is referred to the literature.[66] Helmholtz free energies of adsorption are calculated as

$$A^X_{\mathrm{ads}}(T) = A^X_{\mathrm{H_2O+zeo}}(T) - A^X_{\mathrm{zeo}}(T) - A^X_{\mathrm{H_2O}}(T) \tag{3}$$

where $A^X_{\mathrm{H_2O+zeo}}(T)$ and $A^X_{\mathrm{zeo}}(T)$ were calculated from AIMD calculations, while $A^X_{\mathrm{H_2O}}(T)$ was obtained from static calculations in combination with tabulated values in the NIST chemistry webbook[67] (see Section S4.1 in the SI).

III. RESULTS

III.I. Structure and Relative Stability of Proton Positions in H-SSZ-13. First, we examined the relaxed structures of the H-form of zeolite SSZ-13 after performing geometry optimization using different functionals. In the H-form of SSZ-13, Al−O(H) and Si−O(H) bonds are elongated with respect to the other Al−O and Si−O bonds. To better understand the differences in geometries predicted by various functionals, we first compare the Al−O(H) and Al−O bond lengths. The results are compiled in Table S8 of Section S3. All functionals predict an Al−O(H) bond length between 1.88 and 1.94 Å. The inclusion of dispersion interactions has a negligible effect on the geometry around the active site, and all dispersion-inclusive schemes induce a small elongation of the Al−O(H) bond by at most 0.01 Å compared to equivalent approaches without dispersion corrections (PBE, revPBE). Most structures are similar for all functionals and protonation sites, except for BEEF−vDW and the structure protonated on the O2 position, where the BAS points toward the zeolite cage (Figure 2).

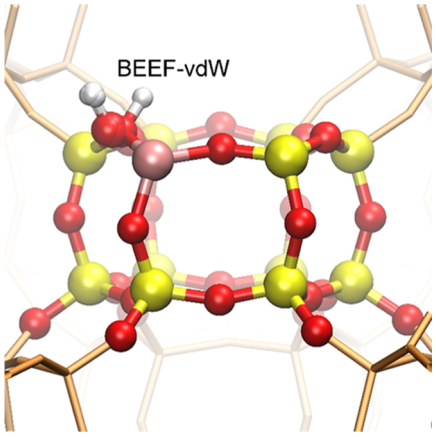

Figure 2. Overlayed relaxed structures of the H-form of zeolite SSZ-13 protonated on the O2 oxygen atom using the following functionals: PBE,[55] PBE-D2,[25,55] PBE-D3,[26,55] revPBE,[56] revPBE-D3,[26,56] vdW-DF,[31] vdW-DF2,[33] optB88-vdW,[32] BEEF−vdW,[34] and rVV10.[36] The structures are identical except the final BEEF−vdW geometry that predicts a different orientation of the BAS than the others. The color code corresponds to Figure 1. Beige lines represent periodic images of the unit cell repeated in each direction.

As a next step, we compare the relative stability between the four different proton positions with respect to the GGA exchange−correlation functional and find that in most cases the variation in relative energy is smaller than 5 kJ/mol, and only BEEF−vdW shows larger differences (O2, Table 1). Nevertheless, this small variation in the relative stability of different proton positions leads to changes in their energetic ordering. Both the PBE and revPBE functionals predict the

https://doi.org/10.1021/acs.jpcc.1c04270
J. Phys. Chem. C 2021, 125, 20261−20274

Table 1. Relative Stabilities (in kJ/mol) for the Four Different Possible Protonation Sites (O1−O4) in Zeolite H-SSZ-13 Computed Using Different Functionals and Methods (RPA and MP2)

	O1	O2	O3	O4
PBE	0.0	2.9	10.1	9.0
revPBE	0.0	2.7	10.3	8.7
PBE-D2	0.0	2.9	7.6	10.4
PBE-D3	0.0	2.9	8.2	9.8
revPBE-D3	0.0	2.7	9.0	9.3
vdW-DF	0.0	4.0	9.1	11.2
vdW-DF2	0.0	4.9	9.6	12.1
optB88-vdW	0.0	3.5	8.1	11.0
BEEF−vdW	0.0	16.0	9.8	11.3
rVV10	0.0	3.5	8.8	10.8
B3LYP-D3	0.0	7.5	9.4	13.5
MP2	0.0	6.7	9.4	12.5
RPA	0.0	6.0	8.9	11.9

stability of protonation sites in the decreasing order O1 (the most stable) → O2 → O4 → O3 (the least stable). The inclusion of dispersion interactions at both PBE-D and vdW-DF levels changes relative stabilities compared to the PBE and revPBE functionals within a margin of 2.5 kJ/mol and makes the protonation on the O3 site favorable over the O4 site. In agreement with RPA and MP2, dispersion-inclusive approaches predict the protonation in the O1 position as most favorable, followed by O2, O3, and O4 positions, with a maximum energy difference between the most and least stable protonation sites of 12.1 kJ/mol (VdW-DF2, Table 1). The exception is the BEEF−vdW functional, which predicts the O2 position to be the least stable (instead of the O4 position). The relaxed BEEF−vdW geometry of O2 is qualitatively very different from the structures obtained from other functionals (see Figure 2), which is consistent with differences in relative stabilities for these sites. The hybrid B3LYP-D3 functional similarly disfavors the O2 protonation site but less than BEEF−vdW and does not affect energetic ordering of the protonation sites. We note that both MP2 and RPA predict quantitatively the same results with a maximum difference in relative stabilities of protonation sites below 1 kJ/mol. These results imply that the effect of dispersion corrections on the stability of the Brønsted acid proton is small, but we find differences in the ordering of the protonation sites compared to the previous work of Göltl et al. who examined energy differences between protonation sites in a similar manner.[42] Such differences could be caused by differences in local strain at the different O atoms, as indicated by the variance in Al−O(H) bond distances and the ability of the zeolite framework to accommodate the additional strain.

III.II. Structure of Water−Zeolite Complexes. After water is adsorbed into the zeolite framework, it can be either physisorbed in the zeolite pore, interact with a BAS, or bind to an Al atom. First, we focus on physisorption. Here, the water molecule can interact with the framework of the all-silica CHA *via* dispersion interactions, which leads to a flat potential energy surface with many degenerate configurations. Figure S1 in the SI shows that each functional predicts a different structure of the adsorbate. We furthermore focus on the minimum Si−O_w distance to describe the position of water in the zeolite pore, and all Si−O_w values are given in Table S9 of the SI. In purely siliceous SSZ-13, the water molecule is in the middle of the cage with the smallest Si−O_w distances ranging from 3.32 to 3.71 Å, depending on the functional used. The exception is the structure optimized using the revPBE functional, where we find a Si−O_w distance of 4.41 Å, which indicates a weaker attraction of the water molecule to the zeolite walls compared to the other functionals. The addition of dispersion interactions at the -D level contracts the minimum Si−O_w by up to 0.71 Å (revPBE-D3), with PBE-D2 leading to the shortest Si−O_w distances (3.31 Å).

Next, we examine water adsorption on the BAS where a strong bond is formed between the acid site and the water oxygen atom (H···O_w) and the acidic proton remains attached to the framework. Except for BEEF−vdW, the bond is always shortest for the O3 protonation site, and the energy ordering of the different bond lengths depends on the choice of the DFT method (Table 2). Comparing the optimized structures reveals that most functionals lead to a similar structure of all water−zeolite complexes and only the revPBE functional leads to significant differences for the O2 protonation site (Figure 3). The addition of dispersion schemes at PBE-D or vdW-DF level does not lead to significant changes in the structures (Figure 3). We find that the choice of functional seems to influence the BAS-proton water bond length more than the addition of dispersion interactions. The PBE functional leads to the shortest distances between water and the Brønsted acid proton (H···O_w = 1.32−1.46 Å), and the addition of -D dispersion corrections induces a further contraction of the H···

Table 2. Relaxed Geometries of Water Adsorbed on a BAS in Zeolite SSZ-13 for All Four Protonation Sites (O1−O4)[a]

	O1		O2		O3		O4	
	H···O_w	H−O_f	H···O_w	H−O_f	H···O_w	H−O_f	H···O_w	H−O_f
PBE	1.46	1.06	1.46	1.07	1.32	1.13	1.45	1.07
revPBE	1.51	1.04	1.50	1.05	1.45	1.07	1.51	1.05
PBE-D2	1.46	1.06	1.45	1.08	1.27	1.16	1.45	1.07
PBE-D3	1.47	1.05	1.46	1.07	1.29	1.15	1.46	1.07
revPBE-D3	1.51	1.04	1.55	1.04	1.45	1.07	1.53	1.05
vdW-DF	1.59	1.02	1.66	1.01	1.57	1.03	1.61	1.03
vdW-DF2	1.60	1.02	1.64	1.02	1.56	1.03	1.61	1.03
optB88-vdW	1.50	1.04	1.50	1.06	1.38	1.10	1.49	1.06
BEEF−vdW	1.54	1.02	1.62	1.02	1.55	1.03	1.67	1.01
rVV10	1.51	1.04	1.50	1.06	1.39	1.09	1.49	1.06

[a]To characterize the geometries, two characteristic distances were used, namely, the H···O_w hydrogen bond length and the distance between the BAS and the protonation site (H−O_f). The distances are given in Å.

https://doi.org/10.1021/acs.jpcc.1c04270
J. Phys. Chem. C 2021, 125, 20261−20274

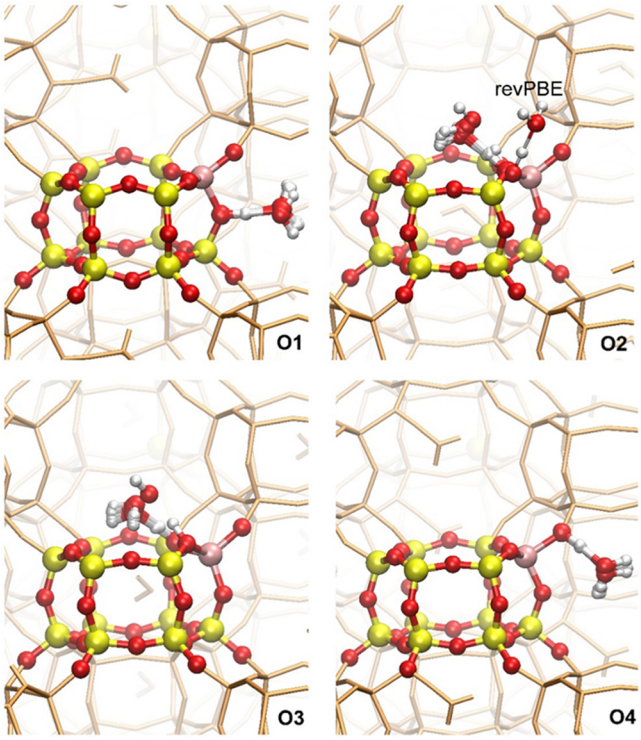

Figure 3. Visual representation of relaxed water−zeolite complexes after water adsorption on the BAS in zeolite SSZ-13 for all four protonation sites (O1−O4). All methods predict structurally similar geometries except the revPBE functional for adsorption on the O2 site. The color code corresponds to Figure 1. Beige lines represent periodic images of the unit cell repeated in each direction.

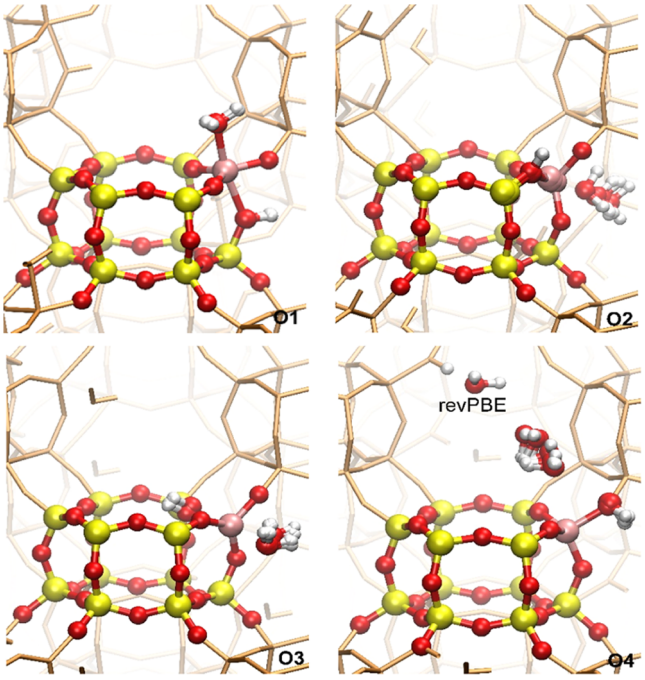

Figure 4. Visual representation of relaxed water−zeolite complexes after the water adsorption on the LAS (the Al atom) in zeolite SSZ-13 for all four protonation sites (O1−O4). All methods predict structurally similar geometries except the revPBE functional for adsorption on the O4 site. The color code corresponds to Figure 1. Beige lines represent periodic images of the unit cell repeated in each direction.

O_w bond of up to 0.05 Å. Interestingly, the opposite effect, *i.e.*, an elongation of the BAS-proton water bond, is observed when applying -D dispersion corrections to the revPBE functional. A similar picture is shown for distances between the water molecule and Si atoms, where the shortest Si−O_w distances fall within the range of 3.45−3.76 Å and the addition of the vdW correction does not induce a change greater than 0.07 Å (Table S9).

In the next step, we investigate the direct adsorption of water on the Al atom in the *anti*-position to the BAS (*i.e.*, on the LAS). Since direct interactions between water and the Al atom can change the bond lengths between Al and the other framework atoms,[20,22] we describe the adsorption complex by two bonds, namely, the Al−O_w and Al−O_f(H) distances. The adsorption complexes are shown in Figure 4, and the numerical values are summarized in Table 3. We find that in most cases water directly binds to the Al atom and the Al−O_w distance lies between 2.05 and 2.28 Å.

Here, the Al−O_f(H) bonds are also elongated by about 0.18−0.28 Å. In most cases, the addition of dispersion corrections at any level has only a negligible effect on the structure of the adsorbed water molecule. However, for some functionals and for the BAS (the proton) located in the O2 or O4 position, Al−O_w distances are larger than 2.5 Å and the Al−O_f(H) distances are almost unchanged. This indicates that water cannot form a chemical bond with the Al atom and is only physisorbed. This is most pronounced for the revPBE and BAS position O4, where we could not find a stable minimum for water close to the Al atom (Figure 4). We have excluded this geometry from further analysis. Furthermore, we find the shortest Si−O_w distances in the range between 3.14 and 4.03 Å (Table S8). The large variation is indicative of the significant differences in the bonding mechanism and with it of stable adsorption geometries for this adsorption process.

Finally, we studied the simultaneous adsorption of two water molecules to the BAS located in the O1 position, which lead to two different structures: (i) the formation of neutral complex with a water dimer adsorbed on the BAS *via* the formation of a hydrogen bond and (ii) the transfer of the acidic proton from the zeolite to the water molecule and the formation of a $H_5O_2^+$ ion (see Figure 5). Interestingly, at the PBE level (including PBE-D2 and PBE-D3), only the $H_5O_2^+$ ion is stable, and we could not identify a stable geometry for the neutral complex. Stable geometries for both adsorption complexes were found for all other functionals. Similar findings have been observed by Vener et al., who only observed the formation of the neutral complex using the BLYP functional but not using PBE.[3] We speculate that the reason why different functionals show different structures for an adsorbed water dimer and in some cases do not stabilize specific structures at all is due to differences in how these methods describe the proton-framework and proton-H bond. If the proton-framework bond is predicted to be stronger, a neutral dimer will be formed; if the proton water bond is stronger, a $H_2O_5^+$ ion will be preferred. In both neutral and charged complexes, the dimers are formed by forming a hydrogen bond between the two water molecules. We describe these complexes using three bond lengths (see Scheme S1 in the Supporting Information), namely, the distance between the framework oxygen atom and the proton (H(BAS)−O_f), the distance between the proton and the nearest water oxygen atom (H(BAS)−O_{w1}), and the distances between the H atom in water molecule 1 and the O

https://doi.org/10.1021/acs.jpcc.1c04270
J. Phys. Chem. C 2021, 125, 20261−20274

Table 3. Relaxed Geometries of the Water Molecule Adsorbed on the LAS (the Al Atom) in Zeolite SSZ-13 for All Four Protonation Sites (O1−O4)[a]

	O1		O2		O3		O4	
	Al−O_w	Al−O_f(H)	Al−O_w	Al−O_f(H)	Al−O_w	Al−O_f(H)	Al−O_w	Al−O_f(H)
PBE	2.05	2.16	2.22	2.05	2.12	2.12	2.26	1.91
revPBE	2.09	2.19	3.95	1.91	2.15	2.17	[b]	1.86
PBE-D2	2.06	2.15	2.21	2.05	2.11	2.11	2.28	1.91
PBE-D3	2.05	2.16	2.23	2.05	2.10	2.11	2.28	1.91
RevPBE-D3	2.09	2.19	3.54	1.91	2.14	2.15	4.01	1.89
VdW-DF	2.12	2.20	3.42	1.91	2.18	2.17	3.74	1.88
VdW-DF2	2.11	2.18	3.14	1.92	2.17	2.15	3.74	1.88
opt88B-vdW	2.06	2.15	2.27	2.03	2.10	2.11	2.97	1.88
BEEF−vdW	2.07	2.18	3.03	1.92	2.17	2.14	2.56	1.90
rVV10	2.06	2.16	2.28	2.03	2.10	2.12	2.31	1.90

[a]Al−O_w and Al−O_f(H) distances were used to characterize the structure of water−LAS complexes. The distances are given in Å. [b]We could not find a stable adsorption geometry for this functional.

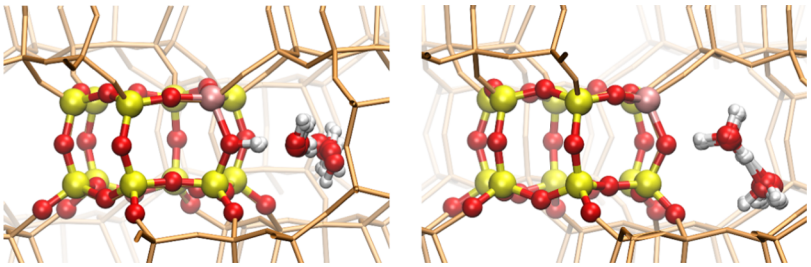

Figure 5. Visual representation of relaxed geometries of two water molecules adsorbed on the BAS bound to the O1 atom in zeolite SSZ-13. Two stable geometries were identified, namely, the formation of a neutral complex in which a water dimer is bound to the BAS *via* hydrogen bond (left) and the formation of a $H_5O_2^+$ ion (right). The neutral complex is not stable for PBE-based approaches, *i.e.*, PBE, PBE-D2, and PBE-D3. Beige lines represent periodic images of the unit cell repeated in each direction.

Table 4. Relaxed Geometries of Two Water Molecules Adsorbed on the BAS Located on the O1 Position in Zeolite SSZ-13[a]

	neutral complex				$H_5O_2^+$ ion			
	H(BAS)−O_f	H(BAS)−O_{w1}	H(O_{w1})−O_{w2}	Al−O_f(H)	H(BAS)−O_f	H(BAS)−O_{w1}	H(O_{w1})−O_{w2}	Al−O_f(H)
PBE					1.44	1.07	1.48	1.80
revPBE	1.08	1.41	1.77	1.87	1.39	1.09	1.55	1.81
PBE-D2					1.48	1.06	1.46	1.80
PBE-D3					1.44	1.07	1.47	1.80
RevPBE-D3	1.09	1.40	1.75	1.87	1.41	1.08	1.53	1.81
VdW-DF	1.04	1.65	1.88	1.88	1.40	1.10	1.61	1.81
VdW-DF2	1.04	1.56	1.83	1.88	1.48	1.07	1.50	1.81
opt88B-vdW	1.11	1.36	1.69	1.85	1.45	1.07	1.50	1.80
BEEF−vdW	1.03	1.54	1.88	1.88	1.48	1.06	1.58	1.81
rVV10	1.11	1.36	1.69	1.86	1.48	1.06	1.50	1.80

[a]Two stable structures were identified: formation of neutral water dimer interacting with the BAS *via* hydrogen bond and formation of a $H_5O_2^+$ ion. Structures were characterized using distances, which are schematically visualized in Scheme S1. The distances are given in Å.

atom of water molecule 2 (H(O_{w1})−O_{w2}). All distances are reported in Table 4. We find that for the neutral complex, the proton is always closer to the framework O atom than to the water molecule, with the shortest H(BAS)−O_f bond lengths for BEEF−vdW, vdW-DF, and vdW-DF2 and the longest bond lengths for optB88b-vdW and rVV10. Reverse trends are found for H(BAS)−O_{w1} bond lengths. For the $H_5O_2^+$ ion, the proton is placed closer to the water molecule and the H(O_{w1})−O_{w2} distance is contracted. At the same time, transfer of the proton to the water dimer leads to a contraction of the Al−O_f(H) bond from 1.85−1.88 to 1.80−1.81 Å.

Summarizing, we find that dispersion-free DFT approaches (PBE and revPBE) predict different relative stabilities of the protonation sites in an empty zeolite SSZ-13 than dispersion-corrected methods. All DFT methods predict a similar structure and bond lengths of an empty zeolite, except BEEF−vdW, which favors a different orientation (and relative stability) of the protonation site on the O2 position. Moreover, we find that all DFT approaches predict quantitatively similar structures if both the BAS and the LAS are well accessible and a strong, either hydrogen (BAS) or donative covalent (LAS), bond is formed between water and the zeolite structure. The PBE functional predicts the shortest binding distances that are unaffected by the addition of -D-type dispersion corrections. The revPBE-based approaches predict the longest binding distances indicating the weakest bonding. Additionally, the

https://doi.org/10.1021/acs.jpcc.1c04270
J. Phys. Chem. C 2021, 125, 20261−20274

revPBE optimization leads to structures that can be very different from all other methods and strongly disfavors the adsorption of water on the Al atom for certain locations of the BAS proton (O2 and O4) that are not well accessible. The addition of vdW dispersion corrections affects the geometry of water−zeolite revPBE complexes and leads to qualitatively different structures from when they are omitted. The bond length of relaxed structures predicted by BEEF−vdW, optB88-vdW, and rVV10 functionals lies between these two extremes but more closely resemble PBE-based structures. The adsorption of two water molecules to the BAS leads to the formation of either a neutral water dimer bonded *via* a hydrogen bond to the BAS or to the formation of a $H_5O_2^+$ ion, in which a proton is transferred to the water molecule. For most methods, both structures are a local minimum, but for PBE-based approaches, only the $H_5O_2^+$ ion is stable.

III.III. Water Adsorption Energies from DFT. Together with the geometrical data of the adsorption complexes, we have analyzed binding strengths calculated using different functionals. The data are summarized in Figure 6 and Table 5.

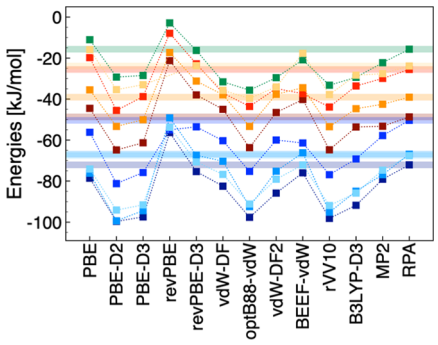

Figure 6. Adsorption energies for one water molecule in zeolite SSZ-13 calculated at different levels of theory. Data are reported for water adsorption to purely siliceous zeolite (green), water adsorption to a BAS in the O1−O4 position (dark to light shades of blue), and water adsorption to the LAS with the BAS in the O1−O4 position (dark red to yellow). Horizontal bars correspond to RPA calculated energies.

First, water adsorption in purely siliceous CHA was studied. Depending on the chosen DFT approach, we find large variations in binding energy. At the revPBE level, there is almost no interaction between the zeolite and water (E_{ads} = −2.84 kJ/mol) as indicated by the large value of the shortest Si−O_w distance (Table S9). Moderate binding is predicted by the PBE functional (E_{ads} = −11.04 kJ/mol). After the addition of vdW corrections, the adsorption becomes more exothermic with E_{ads} between −16.27 and −35.66 kJ/mol, depending on the method used. This is to be expected as water in the siliceous form of SSZ-13 is located in the middle of the zeolite cage with the nearest framework atoms at a distance of about 3.5 Å from the zeolite walls and GGA functionals do not take attractive dispersion interactions into account. The optB88-vdW functional predicts very strong adsorption with an E_{ads} of −35.66 kJ/mol, while revPBE-D3 predicts the weakest binding (E_{ads} = −16.27 kJ/mol). Interestingly, PBE-D2, PBE-D3, and vdW-DF predict a similar adsorption with binding energies of ≈−30 kJ/mol.

The binding energy of water to the BAS varies between −49.15 and −99.61 kJ/mol depending on both the protonation site and the DFT method. All methods predict a preferential adsorption of water to the BAS in the O1 position. Water adsorption is the least favorable to the O2 site and is on average about 20 kJ/mol weaker than to the O1 site. Trends for water adsorbed to the BAS in the O3 and O4 position follow water adsorption to the O1 position and, depending on the used functional, either adsorption to the O3 BAS or the O4 BAS is slightly stronger. RevPBE leads to weakest adsorption with E_{ads} between −49.15 and −56.35 kJ/mol for all four protonation sites.

The dispersion-corrected methods make the adsorption always more exothermic with an average increment in the adsorption energy of −18.09 kJ/mol (revPBE-D3) up to −23.45 kJ/mol (vdW-DF). We note that the adsorption energies of water on the O2 position using the revPBE functional have been omitted from this analysis due to the significant structural differences between the geometries. The average adsorption energies increase in the order: revPBE → revPBE-D3 → BEEF−vdW → PBE → vdW-DF → vdW-DF2 → optB88-vdW → rVV10 → PBE-D3 and PBE-D2, with the latest one being the most binding. The average adsorption energies, as well as individual adsorption energies, are summarized in Table 5.

Table 5. DFT Adsorption Energies (in kJ/mol) of One Water Molecule Adsorbed on the Siliceous Form of Zeolite SSZ-13 or on the BAS (the Proton) and the LAS (the Al Atom) of the H-Form Computed for All Four Protonation Sites (O1−O4)

	Si + H_2O	BAS + H_2O					LAS + H_2O				
		O1	O2	O3	O4	aver.	O1	O2	O3	O4	aver.
PBE	−11.04	−78.62	−56.21	−76.19	−74.15	−71.29	−44.53	−19.79	−35.52	−15.88	−28.93
revPBE	−2.84	−56.35	−55.06	−49.15	−53.74	−53.85	−21.24	−7.92	−17.29	[a]	−15.49
PBE-D2	−29.27	−99.61	−81.23	−99.35	−94.10	−93.57	−64.83	−45.54	−53.34	−35.40	−49.78
PBE-D3	−28.49	−97.45	−75.83	−94.40	−91.57	−89.81	−61.34	−38.80	−50.09	−33.00	−45.81
revPBE-D3	−16.27	−75.39	−53.54	−67.44	−70.68	−66.76	−37.97	−22.82	−31.23	−23.72	−28.94
vdW-DF	−31.60	−82.47	−60.33	−70.35	−76.76	−72.48	−45.01	−37.05	−37.90	−35.74	−38.93
vdW-DF2	−29.57	−85.81	−59.99	−75.20	−79.10	−75.02	−46.55	−34.85	−37.67	−34.11	−38.30
optB88-vdW	−35.66	−97.63	−75.30	−92.41	−91.14	−89.12	−63.72	−43.61	−53.34	−39.67	−50.08
BEEF−vdW	−20.87	−75.98	−61.42	−66.20	−72.13	−68.94	−40.23	−37.39	−34.47	−17.70	−32.45
rVV10	−33.24	−98.15	−76.90	−95.17	−91.87	−90.52	−64.77	−43.88	−53.48	−37.79	−49.98
B3LYP-D3	−29.40	−91.76	−69.22	−84.90	−85.80	−82.92	−53.62	−33.61	−44.71	−28.34	−40.07
MP2	−22.26	−79.11	−57.80	−76.89	−74.69	−72.13	−53.27	−29.93	−42.53	−27.60	−38.33
RPA	−15.67	−72.10	−50.39	−66.88	−67.62	−64.25	−48.72	−25.56	−39.09	−23.87	−34.31

[a]We could not find a stable adsorption geometry for this functional.

https://doi.org/10.1021/acs.jpcc.1c04270
J. Phys. Chem. C 2021, 125, 20261−20274

The adsorption of water on the LAS is always less exothermic than adsorption on the BAS. All methods predict a similar trend, *i.e.*, that the adsorption is strongest to the LAS with the BAS in the O1 position, followed by the O3, O2, and O4 positions. The two functionals that do not follow this trend are BEEF−vdW, where relative stabilities for the BAS in the O2 and O3 positions are switched, and revPBE-D3, where relative stabilities for the BAS in the O2 and O4 positions are switched. We find the weakest adsorption for the revPBE functional with $\overline{E}_{ads}$ = −15.49 kJ/mol, followed by PBE ≈ revPBE-D3 → BEEF−vdW → vdW-DF ≈ vdW-DF2 → PBE-D3 → PBE-D2 → rVV10 and the optB88-vdW functional. Comparing adsorption to the LAS and the BAS reveals that the trends for changes in the adsorption strength between different functionals are similar and also the variation in adsorption strengths between the different adsorption sites.

Two distinct stable adsorption complexes can be formed upon coordination of two water molecules to the BAS: either a neutral water dimer or a $H_5O_2^+$ ion. The adsorption energies are tabulated in Table 6. The corresponding adsorption energies vary between −85.75 kJ/mol (revPBE) and −167.69 kJ/mol (PBE-D2) depending on the functional used. Despite the large energy span, the adsorption for two molecules is always weaker than two times the adsorption of one water molecule to the BAS but stronger than the adsorption of two water molecules to the LAS. Only the nonlocal vdW-DF, vdW-DF2, and BEEF−vdW favor the formation of a neutral water dimer by up to 10 kJ/mol, while all other methods predict the $H_5O_2^+$ ion as a more stable complex. According to PBE-based methods, the neutral complex is never stable.

Table 6. Tabulated Adsorption Energies for the Adsorption of Two Water Molecules on the BAS Bound to the O1 Atom in Zeolite SSZ-13

	neutral complex	$H_5O_2^+$ ion
PBE	[a]	−131.19
revPBE	−85.75	−87.21
PBE-D2	[a]	−167.69
PBE-D3	[a]	−164.27
revPBE-D3	−118.31	−119.68
vdW-DF	−132.03	−124.59
vdW-DF2	−133.35	−128.81
optB88-vdW	−156.56	−161.83
BEEF−vdW	−119.30	−109.92
rVV10	−157.23	−165.03
B3LYP-D3	−135.35	−144.08
MP2	−111.25[b]	−128.08
RPA	−106.79[b]	−112.61

[a]We could not find a stable adsorption geometry for this functional. [b]The adsorption energies were computed using revPBE-D3 structures.

III.IV. Water Adsorption Energies from Hartree−Fock-Inclusive Methods. Although *post*-HF methods, such as RPA or MP2, and hybrid functionals, such as B3LYP-D3, provide more accurate data, for periodic systems, they are typically applied on top of the geometries optimized at the DFT level due to their high computational cost.[42,68] We explored the impact of input structures for RPA by comparing adsorption strengths of one water molecule to the BAS or the LAS. Here, we focused on the proton located in the O1 position and compared adsorption strengths for structures optimized using selected DFT methods. Results are summarized in Table S7. Using RPA, we find average adsorption energies for water adsorption to the BAS of −72.81 kJ/mol and the choice of input structure only has a marginal effect on the observed values (±0.84 kJ/mol). We find a similar behavior for water adsorption on the LAS with a computed adsorption energy of −48.44 ± 0.91 kJ/mol. These results indicate that the obtained results are rather independent of the functional choice for structure optimization, and we have further limited the computation of the adsorption energies to PBE-D3 structures only.

The adsorption energies of one water molecule from RPA and MP2 calculations for both the siliceous CHA and H-form of zeolite SSZ-13 are shown in Figure 6, and numerical values are summarized in Table 5. We find that on average MP2 binds water about 6.02 kJ/mol stronger than RPA. The effect is more pronounced for water binding to the BAS, for which MP2 predicts about 7.88 kJ/mol stronger adsorption, while for water binding to the LAS, the difference is only about 4.02 kJ/mol. Average RPA adsorption energies are −15.67, −64.25, and −34.31 kJ/mol for the adsorption in the siliceous CHA and on the BAS and the LAS in H-SSZ-13, respectively. The average MP2 adsorption energies are −22.26 kJ/mol (siliceous CHA), −72.13 kJ/mol (BAS), and −38.33 kJ/mol (LAS). Both RPA and MP2 predict a favorable water adsorption in siliceous CHA, with RPA being less hydrophilic. RPA adsorption of water on the BAS is about 29.94 kJ/mol more exothermic than on the LAS, which is the lowest energy difference out of all methods. The MP2 energy difference is 33.79 kJ/mol, which is similar to the smallest energy difference obtained from DFT-based methods (vdW-DF). Adsorption energies obtained using the hybrid functional B3LYP-D3 are qualitatively different. Average B3LYP-D3 adsorption energies are significantly more exothermic with −32.41, −82.92, and −40.07 kJ/mol for the adsorption in the siliceous CHA and on the BAS and the LAS in H-SSZ-13, respectively. Additionally, B3LYP-D3 strongly favors water coordination to the BAS, and water adsorption to the LAS is only about 8 kJ/mol more exothermic than water adsorption in hydrophobic siliceous CHA. The results are summarized in Tables 5 and S6 of the SI where also the original (non-CBS adsorption) energies are tabulated.

All three methods indicate the strongest water adsorption in a zeolite with a proton binding to the O1 position, irrespective of the studied binding site. According to RPA and B3LYP-D3, the adsorption energy of water on the BAS decreases in the order O1 → O4 → O3 → O2, while MP2 favors the water adsorption on the BAS on the O3 site over the O4 site. All three methods predict an identical order of adsorption strengths on the LAS with respect to the BAS, namely, O1 → O3 → O2 and O4, with the latter one being the least exothermic.

RPA and MP2, as well as B3LYP-D3, favor the formation of a $H_5O_2^+$ ion over the formation of a neutral water dimer. The adsorption is most exothermic for B3LYP-D3, followed by MP2 and then RPA.

IV. DISCUSSION

It is encouraging to see that all methods agree that water adsorption in purely siliceous zeolite CHA is weakest and water adsorption to the BAS is strongest. At the same time, the relative stability of water upon the adsorption on the BAS or the LAS shows a significant variation between the different functionals. In particular, revPBE predicts very different trends

https://doi.org/10.1021/acs.jpcc.1c04270
J. Phys. Chem. C 2021, 125, 20261−20274

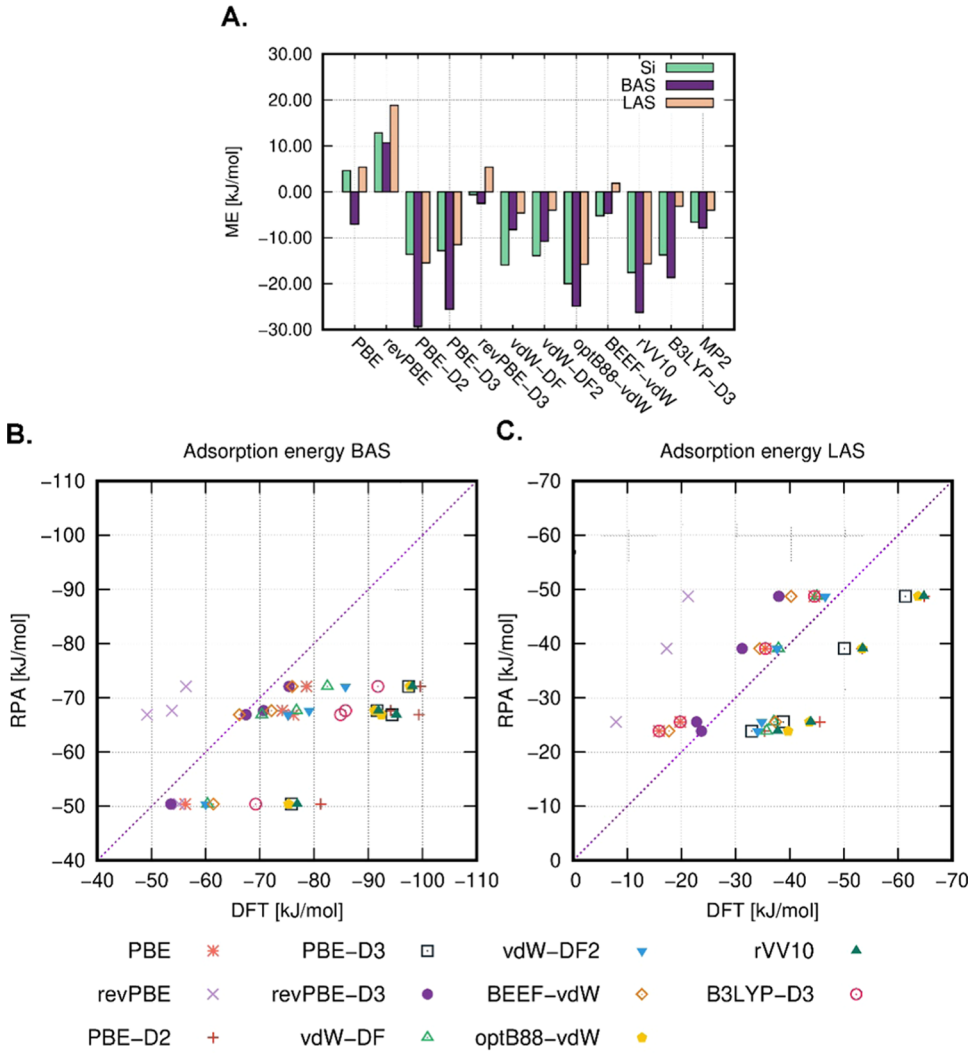

Figure 7. Comparison of DFT-computed adsorption energies of one water molecule in siliceous CHA and in the zeolite H-SSZ-13 with RPA results. (A) Mean errors (MEs) of water adsorption in siliceous CHA (green bars) to the BAS (the proton, violet bars) and the LAS (the Al atom, beige bars) in H-SSZ-13 computed at different levels of theory with respect to RPA calculations. Negative values mean that the method is overbinding compared to RPA, while positive values indicate that the functional is underbinding compared to the reference. Panels (B) and (C) compare individual values for a water molecule adsorbed either on the BAS (the proton, B) or on the LAS (the Al atom, C). Four different protonation sites are possible, creating a set of four different structures for each adsorption type (see Section II.I).

compared to the other functionals, which indicates that this functional, which always shows the weakest adsorption strengths, describes the adsorption processes qualitatively different. Interestingly, the increase in adsorption strength after the addition of dispersion corrections is of a similar order of magnitude for the adsorption of water in all three possible situations, *i.e.*, on the siliceous form of CHA, on the BAS (the proton), or the LAS (the Al atom) of its H-form of zeolite SSZ-13 for each functional, as well as for both -D type of approaches and nonlocal vdW schemes. This agrees with the hypothesis that the potential energy surface resulting from dispersion interactions between water and the zeolite framework is flat and does not depend on the exact configuration of the molecule. When studying the adsorption of two water molecules, we find that most methods agree that the donation of the proton from the framework to the water dimer is favored, and only vdW-DF, vdW-DF2, and BEEF−vdW do not follow this trend.

Beyond a qualitative assessment of the performance of the different methods, another important aspect is to understand how well different functionals can reproduce experimental observations. It is well known that purely siliceous zeolites are hydrophobic at room temperature and do not adsorb water molecules under ambient conditions. To probe which of the methods correctly reproduces this behavior, we calculated the Helmholtz free energies of adsorption of water ($A_{ads}(T)$) in all-silica CHA using *ab initio* molecular dynamics simulations at the revPBE-D3 level and use the results to extrapolate the $A_{ads}(T)$ values for the other functionals. All $A_{ads}(T)$ values are summarized in Figure S2 and Table S10 in the SI. Indeed, $A_{ads}(T)$ values are weakened by about 64 kJ/mol compared to E_{ads}, and all Helmholtz free energies of adsorption are positive (see Figure S2 in the SI). Positive $A_{ads}(T)$ values correspond to hydrophobicity, which agrees well with experimental observations.

While this qualitative agreement with experimental measurements for purely siliceous zeolite SSZ-13 is encouraging, we furthermore want to understand how well the different methods can quantitatively describe water adsorption in zeolite SSZ-13 with a finite Si/Al ratio. However, to the best of our

https://doi.org/10.1021/acs.jpcc.1c04270
J. Phys. Chem. C 2021, 125, 20261−20274

knowledge, no experimental data for the adsorption of one water molecule per Al atom for zeolite SSZ-13 with finite Si/Al ratio are available.

A very common strategy to assess the performance of different DFT methods, when the experimental data are not available, is to compare them to higher-level methods, such as MP2 or RPA calculations, or eventually hybrid functionals such as B3LYP-D3. Previous results for the adsorption of alkanes in zeolites indicate that, in particular, RPA seems to show good agreement with experimental measurements.[42,50] At the same time, it cannot be excluded that MP2 describes the adsorption of water molecules in the protonated form of zeolites better.[20] For the remainder of the discussion, we will therefore compare all DFT results to RPA values as shown in Figures 7 and 8 and give a comparison of DFT results with MP2 in Figures S3 and S4 of the SI.

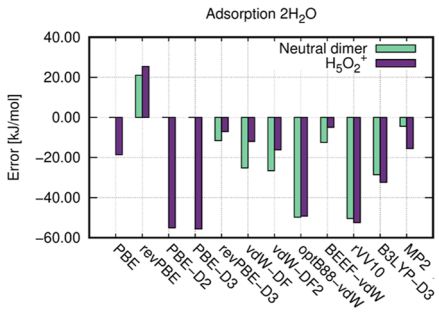

Figure 8. Energy difference for all methods with respect to RPA for the adsorption of two water molecules in H-SSZ-13 with the acidic proton in the O1 position with RPA results. For PBE, PBE-D2, and PBE-D3, no stable structure for the neutral water dimer has been found, and thus for these functionals, the comparison with RPA is made for the $H_5O_2^+$ ion only.

Using this strategy, we find that multiple methods (PBE, revPBE-D3, BEEF−vdW, MP2) exist, which describe all adsorption processes with an error of less than 10 kJ/mol with respect to the RPA adsorption energies. The revPBE functional, on the other hand, is a method that significantly underbinds water for all three adsorption processes, while the remaining methods (PBE-D2, PBE-D3, vdW-DF, vdW-DF2, optB88-vdW, rVV10) overestimate the adsorption strength. While PBE-D2, PBE-D3,optB88-vdW, and rVV10 overestimate the adsorption strength for all adsorption processes, vdW-DF and vdW-DF2 show good agreement with RPA adsorption energies for the LAS site. B3LYP-D3 does not provide qualitatively better results than computationally cheaper GGA methods and is strongly overbinding for water adsorption on the BAS and in siliceous CHA. Using the B3LYP functional without any dispersion corrections might provide better results.

The situation is very different for the adsorption of two water molecules on the BAS. PBE-based methods always favor the formation of a $H_5O_2^+$ ion, and thus comparison with RPA data for the neutral complex is not possible. The binding energies of both complexes are predicted with the smallest error for revPBE-D3 followed by BEEF−vdW with an error of smaller than 13 kJ/mol. The most overbinding methods are PBE-D2, PBE-D3, optB88-vdW, and rVV10 with an error of ∼ 50 kJ/mol.

For the adsorption of one water molecule, the best agreement with RPA data on average is obtained using PBE with an average error of −0.2 kJ/mol. However, PBE overestimates the bond strength of water to the Brønsted proton, while it underestimates the bonding to the zeolite framework and the LAS. This indicates that PBE overestimates the $H-O_w$ bond, while, by construction, it cannot capture dispersion interactions dominating the other adsorption processes accurately. However, the addition of the -D dispersion force field leads to a significant overestimation of the adsorption processes. The combination of the weakly binding revPBE functional with the -D3 force field seems to lead to a favorable description of adsorption with an average deviation of 1.2 kJ/mol from RPA (single water molecule) results. At the same time, BEEF−vdW leads to best agreement with MP2 (see Section S5 of the SI) but deviates from all other models when predicting relative stabilities of the four protonation sites (Table 1). We observe energetic differences of at least 10 kJ/mol for the adsorption of two water molecules, and again revPBE-D3 and BEEF−vdW show best agreement with RPA and MP2 results. Based on this analysis, we recommend using the revPBE-D3 functional to model the adsorption of H_2O in zeolite SSZ-13 since (i) it can qualitatively correctly capture the different contributions to the water adsorption, namely, covalent interactions with the adsorption site and dispersion interactions with the zeolite; (ii) is computationally efficient; (iii) reproduces the adsorption energies of water calculated at RPA and MP2 levels of theory most closely; and (iv) correctly predicts the preference of a $H_5O_2^+$ ion for the adsorption of two water molecules.

V. CONCLUSIONS

We have investigated the adsorption of water in zeolite SSZ-13 using 10 DFT functionals, 1 hybrid functional, and 2 post Hartree−Fock (HF) methods. We studied four different adsorption processes, namely, adsorption of water in purely siliceous CHA, adsorption of water to a Brønsted acid site (BAS), water adsorption to a Lewis acid site (LAS), and the adsorption of two water molecules. We found that all methods predict structurally similar results if the water is strongly bound to a well-accessible BAS or LAS. However, their performance diverges for weak adsorption in siliceous zeolite or on a sterically hindered active site. Adsorption energies show a significant variation of about 50 kJ/mol between the different functionals, but the explicit calculation of Helmholtz free energies of adsorption using AIMD calculations shows that all methods qualitatively predict the experimentally observed hydrophobicity of purely siliceous zeolite SSZ-13. When comparing results from DFT calculations with the more accurate, post-HF methods RPA and MP2, we find that best agreement is found between PBE, revPBE-D3 and RPA, and BEEF−vdW and MP2. It is encouraging to see that the computationally very efficient revPBE-D3 functional can reproduce RPA or MP2 results within 5 kJ/mol, irrespective of the adsorption site. The PBE functional without any dispersion correction predicts similar adsorption energies, but, compared to the revPBE-D3 and the BEEF−vdW approaches, its performance is less consistent with respect to different adsorption sites (BAS, LAS, or a zeolite wall of siliceous SSZ-13). The BEEF−vdW functional reproduces the adsorption energies well but fails to reproduce relative stabilities of the protonation sites and it fails to correctly predict the formation of a $H_5O_2^+$ ion for the adsorption of two water molecules. Based on these considerations, we recommend using the

https://doi.org/10.1021/acs.jpcc.1c04270
J. Phys. Chem. C 2021, 125, 20261−20274

revPBE-D3 functional to model the adsorption of water molecules in purely siliceous or protonated zeolite SSZ-13.

■ ASSOCIATED CONTENT

Supporting Information

The Supporting Information is available free of charge at https://pubs.acs.org/doi/10.1021/acs.jpcc.1c04270.

Unit cell parameters calculated using different DFT functionals, the impact of basis set superposition errors and geometries used for HF-inclusive calculations, the structure of zeolite−water adsorption complexes, details about the calculation of the internal energy and Helmholtz free energy from AIMD, comparison of adsorption energies to MP2, and computational input files for RPA and MP2 calculations

(PDF)

Structural files (ZIP)

■ AUTHOR INFORMATION

Corresponding Author

Florian Göltl − *Department of Biosystems Engineering, University of Arizona, Tucson, Arizona 85721, United States;* orcid.org/0000-0002-7217-0450; Email: fgoeltl@arizona.edu

Authors

Katarina Stanciakova − *Inorganic Chemistry and Catalysis Group, Debye Institute for Nanomaterials Science, Utrecht University, 3584 CG Utrecht, The Netherlands*

Jaap N. Louwen − *Albemarle Catalysts Company BV, 1022 AB Amsterdam, The Netherlands*

Bert M. Weckhuysen − *Inorganic Chemistry and Catalysis Group, Debye Institute for Nanomaterials Science, Utrecht University, 3584 CG Utrecht, The Netherlands;* orcid.org/0000-0001-5245-1426

Rosa E. Bulo − *Inorganic Chemistry and Catalysis Group, Debye Institute for Nanomaterials Science, Utrecht University, 3584 CG Utrecht, The Netherlands;* Present Address: Department of Theoretical Chemistry, Vrije Universiteit Amsterdam, De Boelelaan 1083, 1081 HV Amsterdam, The Netherlands

Complete contact information is available at: https://pubs.acs.org/10.1021/acs.jpcc.1c04270

Notes

The authors declare no competing financial interest.

■ ACKNOWLEDGMENTS

This work was supported by the Netherlands Center for Multiscale Catalytic Energy Conversion (MCEC), an NWO Gravitation program funded by the Ministry of Education, Culture and Science of the government of The Netherlands. The authors also thank The Netherlands Organization for Scientific Research (NWO) for access to the national high-performance computing facilities. F. Göltl acknowledges support from the College of Agriculture and Life Science at the University of Arizona.

■ REFERENCES

(1) Tanabe, K.; Hölderich, W. F. Industrial Application of Solid Acid-Base Catalysts. *Appl. Catal., A* **1999**, *181*, 399−434.

(2) Li, Y.; Li, L.; Yu, J. Applications of Zeolites in Sustainable Chemistry. *Chem* **2017**, *3*, 928−949.

(3) Vener, M. V.; Rozanska, X.; Sauer, J. Protonation of Water Clusters in the Cavities of Acidic Zeolites: $(H_2O)_n$ H-chabazite, n = 1−4. *Phys. Chem. Chem. Phys.* **2009**, *11*, 1702−1712.

(4) Göltl, F.; Love, A. M.; Hermans, I. Developing a Thermodynamic Model for the Interactions between Water and Cu in the Zeolite SSZ-13. *J. Phys. Chem. C* **2017**, *121*, 6160−6169.

(5) Heard, C.; Grajciar, L.; Uhlík, F.; Shamzhy, M.; Opanasenko, M.; Čejka, J.; Nachtigall, P. Zeolite (In)stability under Aqueous or Steaming Conditions. *Adv. Mater.* **2020**, *32*, No. 2003264.

(6) Bordiga, S.; Regli, L.; Lamberti, C.; Zecchina, A.; Bjørgen, M.; Lillerud, K. P. FTIR Adsorption Studies of H_2O and CH_3OH in the Isostructural H-SSZ-13 and H-SAPO-34: Formation of H-Bonded Adducts and Protonated Clusters. *J. Phys. Chem. B* **2005**, *109*, 7724−7732.

(7) Wang, M.; Jaegers, N. R.; Lee, M.-S.; Wan, C.; Hu, J. Z.; Shi, H.; Mei, D.; Burton, S. D.; Camaioni, D. M.; Gutiérrez, O. Y.; et al. Genesis and Stability of Hydronium Ions in Zeolite Channels. *J. Am. Chem. Soc.* **2019**, *141*, 3444−3455.

(8) Perea, D. E.; Arslan, I.; Liu, J.; Ristanović, Z.; Kovarik, L.; Arey, B. W.; Lercher, J. A.; Bare, S. R.; Weckhuysen, B. M. Determining the Location and Nearest Neighbours of Aluminium in Zeolites with Atom Probe Tomography. *Nat. Commun.* **2015**, *6*, No. 7589.

(9) Karwacki, L.; de Winter, D. A. M.; Aramburo, L. R.; Lebbink, M. N.; Post, J. A.; Drury, M. R.; Weckhuysen, M. Architecture-Dependent Distribution of Mesopores in Steamed Zeolite Crystals as Visualized by FIB-SEM Tomography. *Angew. Chem., Int. Ed.* **2011**, *50*, 1294−1298.

(10) Stanciakova, K.; Weckhuysen, B. M. Water−active site interactions in zeolites and their relevance in catalysis. *Trends Chem.* **2021**, *3*, 456−468.

(11) Zhang, L.; Chen, K.; Chen, B.; White, J. L.; Resasco, D. E. Factors that Determine Zeolite Stability in Hot Liquid Water. *J. Am. Chem. Soc.* **2015**, *137*, 11810−11819.

(12) Eckstein, S.; Hintermeier, P. H.; Zhao, R.; Baráth, E.; Shi, H.; Liu, Y.; Lercher, J. A. Influence of Hydronium Ions in Zeolites on Sorption. *Angew. Chem., Int. Ed.* **2019**, *58*, 3450−3455.

(13) Mei, D.; Lercher, J. A. Mechanistic Insights into Aqueous Phase Propanol Dehydration in H-ZSM-5 Zeolite. *AIChE J.* **2017**, *63*, 172−184.

(14) Gounder, R. Hydrophobic Microporous and Mesoporous Oxides as Brønsted and Lewis acid Catalysts for Biomass Conversion in Liquid Water. *Catal. Sci. Technol.* **2014**, *4*, 2877−2886.

(15) Bates, J. S.; Bukowski, B. C.; Greeley, J.; Gounder, R. Structure and Solvation of Confined Water and Water−Ethanol clusters within Microporous Brønsted Acids and Their Effects on Ethanol Dehydration Catalysis. *Chem. Sci.* **2020**, *11*, 7102−7122.

(16) Vjunov, A.; Fulton, J. L.; Camaioni, D. M.; Hu, J. Z.; Burton, S. D.; Arslan, I.; Lercher, J. A. Impact of Aqueous Medium on Zeolite Framework Integrity. *Chem. Mater.* **2015**, *27*, 3533−3545.

(17) Van Speybroeck, V.; Hemelsoet, K.; Joos, L.; Waroquier, M.; Bell, R. G.; Catlow, R. A. Advances in Theory and Their Application within the Field of Zeolite Chemistry. *Chem. Soc. Rev.* **2015**, *44*, 7044−7111.

(18) Chizallet, C. Toward the Atomic Scale Simulation of Intricate Acidic Aluminosilicate Catalysts. *ACS Catal.* **2020**, *10*, 5579−5601.

(19) De Wispelaere, K.; Wondergem, C. S.; Ensing, B.; Hemelsoet, K.; Meijer, E. J.; Weckhuysen, B. M.; Van Speybroeck, V.; Ruiz-Martínez, J. Insight into the Effect of Water on the Methanol-to-Olefins Conversion in H-SAPO-34 from Molecular Simulations and in Situ Micro-spectroscopy. *ACS Catal.* **2016**, *6*, 1991−2002.

(20) Silaghi, M.-C.; Chizallet, C.; Petracovschi, E.; Kerber, T.; Sauer, J.; Raybaud, P. Regioselectivity of Al-O Bond Hydrolysis during Zeolites Dealumination Unified by Brønsted-Evans-Polanyi Relationship. *ACS Catal.* **2015**, *5*, 11−15.

(21) Silaghi, M.-C.; Chizallet, C.; Sauer, J.; Raybaud, P. Dealumination Mechanisms of Zeolites and Extra-Framework Aluminum Confinement. *J. Catal.* **2016**, *339*, 242−255.

(22) Stanciakova, K.; Ensing, B.; Göltl, F.; Bulo, R. E.; Weckhuysen, B. M. Cooperative Role of Water Molecules during the Initial Stage of Water-Induced Zeolite Dealumination. *ACS Catal.* **2019**, *9*, 5119−5135.
(23) Nielsen, M.; Brogaard, R. Y.; Falsig, H.; Beato, P.; Swang, O.; Svelle, S. Kinetics of Zeolite Dealumination: Insights from H-SSZ-13. *ACS Catal.* **2015**, *5*, 7131−7139.
(24) Nielsen, M.; Hafreager, A.; Brogaard, R. Y.; De Wispelaere, K.; Falsig, H.; Beato, P.; Van Speybroeck, V.; Svelle, S. Collective Action of Water Molecules in Zeolite Dealumination. *Catal. Sci. Technol.* **2019**, *9*, 3721−3725.
(25) Grimme, S. Semiempirical GGA-Type Density Functional Constructed with a Long-Range Dispersion Correction. *J. Comput. Chem.* **2006**, *27*, 1787−1799.
(26) Grimme, S.; Antony, J.; Ehrlich, S.; Krieg, H. A Consistent and Accurate Ab Initio Parametrization of Density Functional Dispersion Correction (DFT-D) for the 94 Elements H-Pu. *J. Chem. Phys.* **2010**, *132*, No. 154104.
(27) Becke, A. D. Density-functional exchange-energy approximation with correct asymptotic behavior. *Phys. Rev. A.* **1988**, *38*, 3098−3100.
(28) Lee, C.; Yang, W.; Parr, R. G. Development of the Colle-Salvetti correlation-energy formula into a functional of the electron density. *Phys. Rev. B.* **1988**, *37*, 785−789.
(29) Vosko, S. H.; Wilk, L.; Nusair, M. Accurate spin-dependent electron liquid correlation energies for local spin density calculations: a critical analysis. *Can. J. Phys.* **1980**, *58*, 1200−1211.
(30) Stephens, P. J.; Devlin, F. J.; Chabalowski, C. F.; Frisch, M. J. *Ab Initio* Calculation of Vibrational Absorption and Circular Dichroism Spectra Using Density Functional Force Fields. *J. Phys. Chem. A* **1994**, *98*, 11623−11627.
(31) Dion, M.; Rydberg, H.; Schröder, E.; Langreth, D. C.; Lundqvist, B. I. Van der Waals Density Functional for General Geometries. *Phys. Rev. Lett.* **2004**, *92*, No. 246401.
(32) Klimeš, J.; Bowler, D. R.; Michaelides, A. Chemical Accuracy for the van der Waals Density Functional. *J. Phys.: Condens. Matter.* **2010**, *22*, No. 246401.
(33) Lee, K.; Murray, E.; Kong, L.; Lundqvist, B. I.; Langreth, D. C. Higher-Accuracy van der Waals Density Functional. *Phys. Rev. B* **2010**, *82*, No. 081101(R).
(34) Wellendorff, J.; Lundgaard, K. T.; Møgelhøj, A.; Petzold, V.; Landis, D. D.; Nørskov, J. K.; Bligaard, T.; Jacobsen, K. W. Density Functionals for Surface Science: Exchange-Correlation Model Development with Bayesian Error Estimation. *Phys. Rev. B* **2012**, *85*, No. 235149.
(35) Vydrov, O.; van Voorhis, T. Nonlocal van der Waals Density Functional: The Simpler the Better. *J. Chem. Phys.* **2010**, *133*, No. 244103.
(36) Sabatini, R.; Gorni, T.; de Gironcoli, S. Nonlocal van der Waals Density Functional Made Simple and Efficient. *Phys. Rev. B* **2013**, *87*, 04108.
(37) Cížek, J. On the Correlation Problem in Atomic and Molecular Systems. Calculation of Wave-function Components in Ursell-Type Expansion Using Quantum-Field Theoretical Methods. *J. Chem. Phys.* **1966**, *45*, 4256−4266.
(38) Møller, C.; Plesset, M. S. Note on an Approximation Treatment for Many-Electron Systems. *Phys. Rev.* **1934**, *46*, 618−622.
(39) Bohm, D.; Pines, D. A Collective Description of Electron Interactions: III. Coulomb Interactions in a Degenerate Electron Gas. *Phys. Rev.* **1953**, *92*, 609−625.
(40) Gell-Mann, M.; Brueckner, K. A. Correlation Energy of an Electron Gas at High Density. *Phys. Rev.* **1957**, *106*, 364−368.
(41) Tkatchenko, A.; Scheffler, M. Accurate Molecular van der Waals Interactions from Ground-State Electron Density and Free-Atom Reference Data. *Phys. Rev. Lett.* **2009**, *102*, No. 073005.
(42) Göltl, F.; Grüneis, A.; Bucko, T.; Hafner, J. Van der Waals Interactions Between Hydrocarbon Molecules and Zeolites: Periodic Calculations at Different Levels of Theory, from Density Functional Theory to the Random Phase Approximation and Møller-Plesset Perturbation Theory. *J. Chem. Phys.* **2012**, *137*, No. 114111.
(43) Piccini, G.; Alessio, M.; Sauer, J.; Zhi, Y.; Liu, Y.; Kolvenbach, R.; Jentys, A.; Lercher, J. A. Accurate Adsorption Thermodynamics of Small Alkanes in Zeolites. Ab initio Theory and Experiment for H-Chabazite. *J. Phys. Chem. C* **2015**, *119*, 6128−6137.
(44) Svelle, S.; Tuma, Ch.; Rozanska, X.; Kerber, T.; Sauer, J. Quantum Chemical Modeling of Zeolite-Catalyzed Methylation Reactions: Toward Chemical Accuracy for Barriers. *J. Am. Chem. Soc.* **2009**, *131*, 816−825.
(45) Tuma, C.; Kerber, T.; Sauer, J. The tert-Butyl Cation in H-Zeolites: Deprotonation to Isobutene and Conversion into Surface Alkoxides. *Angew. Chem., Int. Ed.* **2010**, *49*, 4678−4680.
(46) Hansen, N.; Kerber, T.; Sauer, J.; Bell, A. T.; Keil, F. J. Quantum Chemical Modeling of Benzene Ethylation over H-ZSM-5 Approaching Chemical Accuracy: A Hybrid MP2:DFT Study. *J. Am. Chem. Soc.* **2010**, *132*, 11525−11538.
(47) Plessow, P.; Studt, F. Unraveling the Mechanism of the Initiation Reaction of the Methanol to Olefins Process Using ab Initio and DFT Calculations. *ACS Catal.* **2017**, *7*, 7987−7994.
(48) Göltl, F.; Michel, C.; Andrikopoulos, P. C.; Love, A. M.; Hanfer, J.; Hermans, I.; Sauter, P. Computationally Exploring Confinement Effects in the Methane-to-Methanol Conversion Over Iron-Oxo Centers in Zeolites. *ACS Catal.* **2016**, *6*, 8404−8409.
(49) Göltl, F.; Bhandari, S.; Mavrikakis, M. Thermodynamics Perspective on the Stepwise Conversion of Methane to Methanol over Cu-Exchanged SSZ-13. *ACS Catal.* **2021**, *11*, 7719−7734.
(50) Göltl, F.; Hafner, J. Modelling the Adsorption of Short Alkanes in Protonated Chabazite: The Impact of Dispersion Forces and Temperature. *Microporous Mesoporous Mater.* **2013**, *166*, 176−184.
(51) Göltl, F.; Hafner, J. Structure and Properties of Metal-Exchanged Zeolites Studied Using Gradient-Corrected and Hybrid Functionals. I. Structure and Energetics. *J. Chem. Phys.* **2012**, *136*, No. 064501.
(52) Vandevondele, J.; Krack, M.; Mohamed, F.; Parrinello, M.; Chassaing, T.; Hutter, J. Quickstep: Fast and Accurate Density Functional Calculations Using a Mixed Gaussian and Plane Waves Approach. *Comput. Phys. Commun.* **2005**, *167*, 103−128.
(53) Hutter, J.; Iannuzzi, M.; Schiffmann, F.; Vandevondele, J. Cp2k: Atomistic Simulations of Condensed Matter Systems. *Wiley Interdiscip. Rev.: Comput. Mol. Sci.* **2014**, *4*, 15−25.
(54) Krack, M. Pseudopotentials for H to Kr Optimized for Gradient-Corrected ExchangeCorrelation Functionals. *Theor. Chem. Acc.* **2005**, *114*, 145−152.
(55) Perdew, J. P.; Burke, K.; Ernzerhof, M. Generalized Gradient Approximation Made Simple. *Phys. Rev. Lett.* **1997**, *78*, 1396.
(56) Zhang, Y.; Yang, W. Comment on "Generalized Gradient Approximation Made Simple. *Phys. Rev. Lett.* **1998**, *80*, 890.
(57) Murray, É. D.; Lee, K.; Langreth, D. C. Investigation of Exchange Energy Density Functional Accuracy for Interacting Molecules. *J. Chem. Theory Comput.* **2009**, *5*, 2754−2762.
(58) Del Ben, M.; Hutter, J.; VandeVondele, J. Second-Order Møller-Plesset Perturbation Theory in the Condensed Phase: An Efficient and Massively Parallel Gaussian and Plane Waves Approach. *J. Chem. Theory Comput.* **2012**, *8*, 4177−4188.
(59) Del Ben, M.; Schütt, O.; Wentz, T.; Messmer, P.; Hutter, J.; VandeVondele, J. Enabling simulation at the fifth rung of DFT: Large scale RPA calculations with excellent time to solution. *Comput. Phys. Commun.* **2015**, *187*, 120−129.
(60) Del Ben, M.; Hutter, J.; Vandevondele, J. Electron Correlation in the Condensed Phase from a Resolution of Identity Approach Based on the Gaussian and Plane Waves Scheme. *J. Chem. Theory Comput.* **2013**, *9*, 2654−2671.
(61) Guidon, M.; Hutter, J.; VandeVondele, J. Auxiliary Density Matrix Methods for Hartree−Fock Exchange Calculations. *J. Chem. Theory Comput.* **2010**, *6*, 2348−2364.
(62) Helgaker, T.; Klopper, W.; Koch, H.; Noga, J. Basis-set Convergence of Correlated Calculations on Water. *J. Chem. Phys.* **1997**, *106*, 9639−9646.

https://doi.org/10.1021/acs.jpcc.1c04270
J. Phys. Chem. C 2021, 125, 20261−20274

(63) Dunning, T. H., Jr. Gaussian Basis Sets for Use in Correlated Molecular Calculations. I. the Atoms Boron through Neon and Hydrogen. *J. Chem. Phys.* **1989**, *90*, 1007−1023.
(64) Woon, D.; Dunning, T. H., Jr. Gaussian Basis Sets for Use in Correlated Molecular Calculations. III. the Atoms Aluminum through Argon. *J. Chem. Phys.* **1993**, *98*, 1358−1371.
(65) Silaghi, M. C. Ab Initio Molecular Modelling of the Dealumination and Desilication Mechanisms of Relevant Zeolite Frameworks. Ph.D. Thesis, Ecole Doctorale de Chimie de Lyon, 2014.
(66) Göltl, F.; Conrad, S.; Wolf, P.; Müller, P.; Love, A. M.; Burt, S. P.; Wheeler, J. N.; Hamers, R. J.; Hummer, K.; Kresse, G.; et al. UV−Vis and Photoluminescence Spectroscopy to Understand the Coordination of Cu Cations in the Zeolite SSZ-13. *Chem. Mater.* **2019**, *31*, 9582−9592.
(67) Afeefy, H. Y.; Liebman, J. F.; Stein, S. E. *Neutral Thermochemical Data*, https://doi.org/10.18434/T4D303 in NIST Chemistry WebBook, NIST Standard Reference Database Number 69; Linstrom, P. J.; Linstrom, P. J.; Mallard, W. G., Eds.; National Institute of Standards and Technology: Gaithersburg MD, retrieved April 11, 2021; 20899.
(68) Paolucci, Ch.; Parekh, A. A.; Khurana, I.; Di Iorio, J. R.; Li, H.; Caballero, J. D. A.; Shih, A. J.; Anggara, T.; Delgass, W. N.; Miller, J. T.; et al. Catalysis in a Cage: Condition-Dependent Speciation and Dynamics of Exchanged Cu Cations in SSZ-13 Zeolites. *J. Am. Chem. Soc.* **2016**, *138*, 6028−6048.

https://doi.org/10.1021/acs.jpcc.1c04270
J. Phys. Chem. C 2021, 125, 20261−20274